

Reduction and immobilization of chromium(VI) by iron(II)-treated faujasite

Jon R. Kiser, Bruce A. Manning*

Department of Chemistry and Biochemistry, San Francisco State University, 1600 Holloway Avenue, San Francisco, CA 94132, USA

ARTICLE INFO

Article history:

Received 2 June 2009

Received in revised form 4 September 2009

Accepted 7 September 2009

Available online 15 September 2009

Keywords:

Chromium(VI)

Chromium(III) iron

Zeolite

Faujasite

X-ray

ABSTRACT

Removal of hexavalent chromium (Cr(VI)) from wastewater typically involves reduction of Cr(VI) to insoluble Cr(III) using zerovalent iron (Fe⁰) or ferrous iron (Fe(II)). This study investigates the effectiveness of Fe(II)-treated faujasite (zeolite Fe(II)-Y) for reduction of Cr(VI) and immobilization (adsorption/co-precipitation) of the Cr(III) reaction product. The Fe(II)-faujasite material effectively removed high concentrations of dissolved Cr(VI) from aqueous solution resulting in Cr solid loadings as high as 0.30 mmol Cr per gram Fe(II)-faujasite or ~1.5% Cr (w:w). Results of Cr K-edge X-ray absorption near edge spectroscopy (XANES) confirmed that the oxidation state of Cr in Cr(VI)-treated Fe(II)-faujasite was Cr(III). The local atomic structure of Cr was investigated by extended X-ray absorption fine structure (EXAFS) spectroscopy and the structure of Cr in the product was described by a Cr–O first shell of six O atoms at 1.98(±0.02) Å plus a second atomic shell of metal (Cr, Fe) at 3.13(±0.02) Å. The EXAFS results, combined with SEM imaging and X-ray diffraction analyses, suggested that the product of the reaction of Cr(VI) with Fe(II)-faujasite is primarily a poorly ordered Cr_xFe_{1-x}(OH)₃ mixed phase similar to previous investigations of the reaction of Cr(VI) with Fe⁰ and not solely Cr(III) bound directly to zeolite cation exchange sites.

© 2009 Elsevier B.V. All rights reserved.

1. Introduction

Chromium(VI) is a toxic contaminant found in electroplating, leather tanning, pulp production, metal finishing, paint, and petroleum refining wastes. Contamination of the environment with Cr(VI) is a potential concern due to both the toxicity of Cr(VI) [1–4] and the mobility of the Cr(VI) in soil, subsurface groundwater, and landfill environments [5,6]. Chromium exists in both the Cr(III) and Cr(VI) oxidation states in the environment. The Cr(III) species is not highly mobile in soil due to precipitation of insoluble Cr(OH)₃ and CrOOH solid phases and adsorption on soil mineral surfaces [7–9]. In contrast, the Cr(VI) species is a soluble anion (Cr₂O₇²⁻ or CrO₄²⁻) with relatively poor affinity for mineral surfaces [3,10,11].

Remediation of dissolved Cr(VI) from contaminated water has received extensive study [12–23]. Several investigations of Cr(VI) reactions with iron species, including ferrous iron (Fe(II)), iron sulfide, and zerovalent iron (Fe⁰), have proven effective for reduction of Cr(VI) to Cr(III) [14–25]. The products of the Fe(II)–Cr(VI) and Fe⁰–Cr(VI) reactions are believed to be amorphous Fe(III)–Cr(III) hydroxide mixed solid phase (Cr_xFe_{1-x}(OH)₃) [15,16,22,23,26–28]. Additionally, the presence of Fe(III) hydroxide and amorphous silica have been shown to accelerate reduction of Cr(VI) by Fe(II) [29,30]. The most effective substrates for remediation of Cr(VI) must both

reduce Cr(VI) to Cr(III) and bind the Cr(III) product to minimize the possibility of subsequent remobilization. Subsequent re-oxidation of Cr(III) back to Cr(VI), as can occur by the reaction of Cr(III) with soil manganese oxide compounds [31] must be avoided.

The approach investigated in the current study employs Fe(II) as a Cr(VI) reductant and zeolite as a solid phase support for binding cations (Fe²⁺, Fe³⁺, and Cr³⁺) and providing sites for precipitation of Fe(III) and Cr(III) hydroxides. Zeolites are micro- and nano-porous aluminosilicates that are widely employed for cation exchange, catalysis, and remediation of metals in wastewaters [32–34]. The CrO₄²⁻ anion is not strongly adsorbed on un-modified zeolite due to permanent, structural negative charge of the crystal lattice [35]. However, cationic surfactant-modified zeolite has been shown to be an effective Cr(VI) adsorbent [36–39]. The Cr(III) cation is strongly adsorbed by a variety of natural and synthetic zeolites [34].

In the current study we investigate the reaction of Cr(VI) with Fe(II)-exchanged faujasite. A variety of experimental techniques were employed including equilibrium batch reactions, competitive Cr(III)/Fe(II) experiments, and several X-ray techniques for elucidation of the chemical characteristics of the products. The objectives of this study were to (1) evaluate the Cr(VI) reduction capacity of Fe(II)-exchanged zeolite, (2) investigate the elemental composition, morphology, crystallography, and structural atomic environment of Cr in the products, and (3) develop a conceptual model for the mechanism of Cr(VI) reduction and Cr(III) immobilization by the Fe(II)-faujasite material.

* Corresponding author. Tel.: +1 415 338 1292; fax: +1 415 338 2384.
E-mail address: bmanning@sfsu.edu (B.A. Manning).

2. Experimental

2.1. Materials

All chemicals in this study were reagent grade (FeCl_2 , CrCl_3 , Na_2CrO_4 , HCl) and all solution preparations employed deionized (DI) water. Sodium-exchanged faujasite (zeolite-Y, or NaY) powder was used in this study (Zeolyst International CBV100, $\text{SiO}_2/\text{Al}_2\text{O}_3 = 5.1$, Na form). The NaY material is a calcined, synthetic zeolite containing a sodalite secondary building unit (truncated cubo-octahedron) with a high surface area ($\geq 500 \text{ m}^2 \text{ g}^{-1}$) and an effective channel width of 7.4 \AA [40] capable of accepting hydrated cations (Cr^{3+} , Fe^{3+} , and Fe^{2+}) and anions (CrO_4^{2-}) into interior channel sites. The Na-Y material was used without additional preparation or purification.

2.2. Fe(II), Fe(III), Cr(III), and Cr(VI) batch reactions

Adsorption reactions employed a reciprocating shaker (100 rpm) and were conducted using $50.0(\pm 0.1) \text{ mg}$ zeolite solid in $20.0(\pm 0.1) \text{ mL}$ solution volumes contained in 50 mL polycarbonate centrifuge tubes at room temperature ($22 \pm 1 \text{ }^\circ\text{C}$). A preliminary investigation determined that 48 h was adequate time for equilibration of the zeolite solid-solution mixtures and thus all batch reactions were terminated at 48 h. Samples were centrifuged at 8000 rpm for 10 min, decanted, and filtered through $0.2 \text{ }\mu\text{m}$ membrane disks to remove particulates. Total dissolved metal (Fe and Cr) analyses were performed by flame atomic absorption spectrometry (FAAS) with a Varian 220FS spectrometer. In all batch experiments equilibrium solution pH was measured for determination of activities, speciation, and solubility limits.

Treatment of faujasite with Fe(II), Fe(III), and Cr(III) involved dissolving and diluting FeCl_2 , FeCl_3 , and CrCl_3 salts in 0.001 M HCl to prevent precipitation. The Fe(II) solutions were prepared fresh prior to each experiment to prevent oxidation of Fe(II) to Fe(III). Both single ion (Fe(II) and Cr(III)) and dual ion experiments were performed. Dual ion experiments were performed either as simultaneous (Fe(II) + Cr(III)) or sequential (Fe(II) \rightarrow Cr(III), Cr(III) \rightarrow Fe(II), and Cr(III) \rightarrow Fe(III)) ion additions. For sequential experiments, reaction mixtures (50 mg faujasite solid in 20 mL solution) were allowed to equilibrate by shaking 48 h followed by removal of the first ion solution (centrifuge, vacuum decant, filter) and replacement with the second ion solution. After 48 h shaking the second solution was removed, filtered, and immediately analysed for total Cr and Fe concentration by FAAS.

The equilibrium Fe(II) adsorption isotherm (see Fig. 1) was used to evaluate the maximum Fe(II) uptake by faujasite. A maximum loading of 1.05 mmol/g was shown to be reproducible and was chosen for further reaction studies with Cr(VI). The Cr(VI) reaction experiments were conducted by first centrifuging the Fe(II)-treated faujasite (8000 rpm for 10 min), decanting excess Fe(II) solution from solid pellets, and rinsing once with 0.001 M HCl. The solids were then resuspended in 20 mL of varying dissolved Cr(VI) concentration (0–1.8 mM) and allowed to react for 48 h followed by analysis of total Fe and Cr in solution by FAAS.

2.3. SEM-EDX and XRD analyses

Imaging of the reacted faujasite solids was performed with a Zeiss Ultra 55 field emission scanning electron microscope (SEM) equipped with a Gemini FEG column. Samples were mounted on Al stubs with carbon tape. Images were collected with a secondary electron in-lens detector. Elemental composition was analysed by energy-dispersive X-ray (EDX) analyses with an Oxford X-Max Si drift detector at a working distance of 10 mm, accelerating voltage of 13 keV, 35° take-off angle, and a count rate of 10,000 cps. This

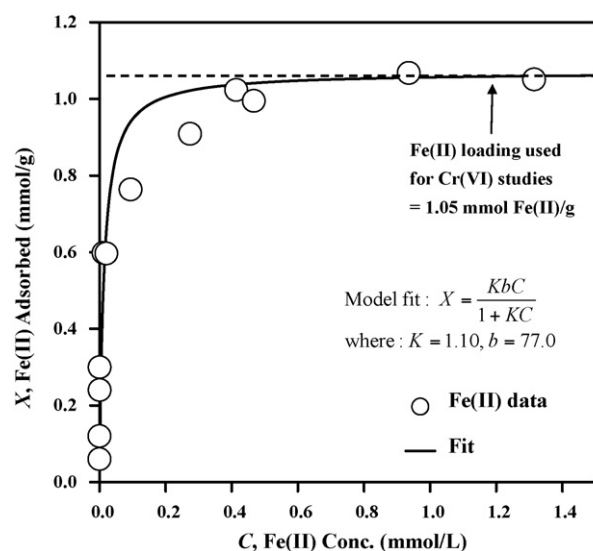


Fig. 1. Measured Fe(II) on faujasite adsorption isotherm and Langmuir model least-squares fit (solid curve). The dotted line indicates the Fe(II) treatment level (1.05 mmol/g) used for further experiments with Cr(VI).

provided an X-ray resolution of 126 eV (FWHM). The crystallography of the untreated (Na form), Fe(II)-, Cr(III)-, and Cr(VI)-treated Fe(II)-faujasite was investigated with a Bruker D8 ADVANCE X-ray diffractometer using a $\text{Cu K}\alpha$ source (40 keV), Bragg-Brentano primary beam optics (slit width 1.0 mm), and scan parameters from 10 to $100^\circ 2\theta$ at $0.05^\circ 2\theta$ increments. The faujasite samples analysed by SEM-EDX and XRD were identical in preparation to those described below for X-ray absorption spectroscopy.

2.4. X-ray absorption spectroscopy

Samples for XAS analysis were prepared in four batches of 2.5 g of Fe(II)-faujasite powder (1.0 L 200 mg/L Fe(II) in 1 L HDPE bottles). After 48 h shaking the solids were collected by vacuum filtration with 47 mm diameter $0.2 \text{ }\mu\text{m}$ filter-disks, and the filtrate reserved for metals analysis by FAAS. The wet paste samples were rinsed with $50\text{--}100 \text{ mL}$ DI water, divided into three aliquots, weighed, and the individual portions transferred to 500 mL HDPE bottles for immediate treatment with 333 mL of 0.85 mM Cr(III) or Cr(VI). After 48 h shaking, the solids were again recovered as a wet pastes with the filtrate analysed for total Cr and Fe by FAAS. The wet paste samples were stored on the filter-disks for 3 days in Ar-purged plastic centrifuge tubes prior to XAS analysis.

The XAS measurements were conducted at the GeoSoilEnviro-CARS facility, beamline 13BM-D, at Argonne National Laboratory's Advanced Photon Source (APS). Several model compounds were measured to provide reference data, including Cr metal foil for energy calibration, Cr(VI)-treated Fe oxyhydroxide (FeOOH), Cr salts (Na_2CrO_4 and CrCl_3), and Cr solutions. Zeolite, Cr salt, and Cr solution samples were mounted in $24 \text{ mm} \times 5 \text{ mm}$ slots cut in 2 mm thick plexiglass sample-holders with Kapton tape. Both Cr and Fe K-edge absorption spectra were collected. The Cr and Fe X-ray absorption edges were scanned from $5860\text{--}6370 \text{ eV}$ (Cr) and $6980\text{--}7500 \text{ eV}$ (Fe). Energy step intervals were 0.5 eV within -20 to $+20 \text{ eV}$ of the edge step (XANES region) and 1.0 eV in the extended (EXAFS region). X-ray energy was controlled with a $\text{Si}(111)$ monochromator. The K-edge absorption spectra were collected as X-ray fluorescence using a Canberra 16 element Ge solid-state multielement detector, with the samples mounted at a 45° angle to the incident beam. Incident beam energy (I_0) was recorded using a standard N_2 ionization detector. In all cases eight

scans per sample were collected. The potential for photoreduction of Cr(VI) by the X-ray beam was assessed by performing a time series measurement on a reference Cr(VI) solution. No photoreduction of Cr(VI) was detectable over the timescale of our measurement runs.

Analysis of EXAFS and XANES data were performed using SIXPACK [41] and IFEFFIT [42] software. Individual scans were averaged, the linear pre-edge was subtracted, and the absorption post-edge step was normalized for all samples. The EXAFS spectrum was produced by isolation of the $\chi(k)$ function with a cubic spline function followed by k^3 weighting. Theoretical EXAFS amplitude and phase functions for Cr–O, Cr–Cr, Cr–Si, and Cr–Fe single scattering paths were generated by FEFF 8.0 [43]. Fitted parameters such as amplitude reduction factor (S_0^2), Fermi shift (E_0), inter-atomic distance (R), and Debye–Waller factor (σ^2) were fitted in k -space. The Cr–O shell coordination number (N) was held constant at $N=4$ for Cr(VI) and $N=6$ for samples containing Cr(III). The S_0^2 was initially established as 0.8 by fitting of a 2.0 mM Na_2CrO_4 solution EXAFS spectrum with fixed values of $N=4$ O atoms and $R_{\text{Cr-O}} = 1.69 \text{ \AA}$. Fitting of subsequent spectra used $S_0^2 = 0.8$ as a starting value followed by adjusting this parameter as a final step in the fit. The quality of the overall fits were calculated using the following goodness of fit parameter

$$\text{Fit}(\%) = \left(\frac{\sum(\chi_{\text{exp}} - \chi_{\text{fit}})^2}{\sum(\chi_{\text{exp}})^2} \right) \times 100 \quad (1)$$

where χ_{exp} and χ_{fit} are the experimental and calculated $\chi(k)$ function data, respectively. Errors in fitted parameters generated in SIXPACK output were $\pm 0.02 \text{ \AA}$ for R and $\pm 20\%$ for N .

3. Results and discussion

3.1. Fe(II) and Cr(III) uptake by faujasite

Cation exchange of faujasite was explored under a variety of conditions for Fe(II) and Cr(III). Equilibrium single ion and sequential ion exchange isotherm data were measured and used to determine the adsorption capacities by fitting with a Langmuir adsorption model

$$C_s = \frac{S_m K C_L}{1 + K C_L} \quad (2)$$

where C_s is the amount of adsorbed solute, C_L the equilibrium solute concentration, K and S_m are constants representing the solute affinity and maximum adsorption capacity, respectively. The Langmuir fitted parameters are provided in Figs. 1 and 2 along with the experimental data. The Fe(II) uptake on faujasite displayed a steep, high-energy uptake region (0–0.6 mmol Fe(II)/g) at low Fe(II) coverage which reached a maximum at $S_m = 1.10$ mmol Fe(II) per gram faujasite (Fig. 1). The Langmuir fit was not ideal in the equilibrium dissolved Fe(II) concentration range between 0.2 and 0.5 mM. However a satisfactory fit was accomplished at lower coverage (0–0.6 mmol Fe(II)/g) and higher coverage near the adsorption maximum. The Fe(II)–faujasite used for Cr(VI) treatment studies contained 1.05 mmol Fe(II) per gram faujasite.

Results of Cr(III) uptake by untreated faujasite are shown in Fig. 2. The goal of this experiment was to confirm that Cr(III) (the Cr(VI) reduction product) was effectively adsorbed by faujasite. Since Cr(III) solubility is pH dependent, the solubility limits were calculated using the measured equilibrium pH of 3.3 to confirm that the Cr(III) removal was an adsorption process rather than precipitation of $\text{Cr}(\text{OH})_3$. For the results in Fig. 2 the calculated solubility limit for Cr(III) was approximately 100 times greater than the measured Cr(III) concentrations at equilibrium. The impact of pH on Fe(II) and Cr(III) uptake was also evaluated indicating a relatively small

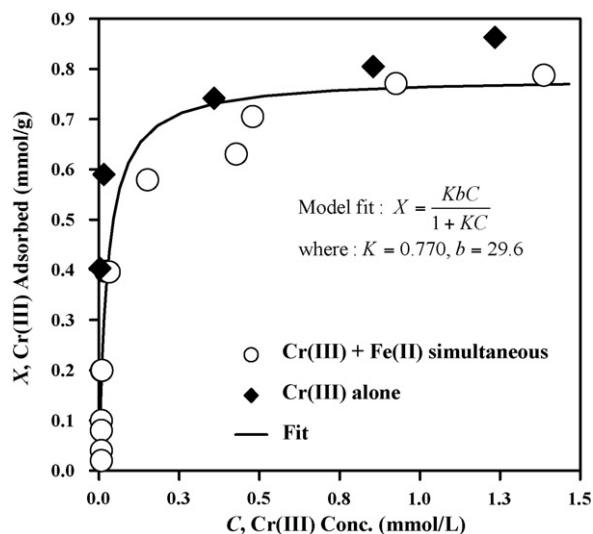


Fig. 2. Measured Cr(III) isotherms and Langmuir model least-squares fit. Data presented are for simultaneous, dual ion Cr(III) + Fe(II) uptake (Cr:Fe mole ratio = 0.67) and single ion Cr(III). The Langmuir isotherm least-squares fit includes both data sets.

competitive influence by H^+ (data not shown). On a charge equivalents basis, the observed adsorption capacity for Cr(III) by faujasite was equal to, or slightly higher than that for Fe(II), depending only slightly on pH within the pH range studied (pH 3–4). In addition, Cr(III) adsorption was nearly independent of Fe(II) concentration over a wide [Fe(II)] range. Measurements using simultaneous, competitive uptake of Fe(II) and Cr(III) on faujasite (Fig. 2) indicate a significantly higher affinity for Cr(III) than for Fe(II), consistent with the higher coulombic potential of the trivalent Cr^{3+} cation.

The results of sequential treatments (Fig. 3) indicated that most of the Fe(II) was displaced by Cr(III)–exchange. In these experiments faujasite was loaded with cation (either Fe^{2+} or Cr^{3+}) to the adsorption maxima prior to addition of the second cation. Sequential treatment with Cr(III) followed by Fe(II) displaces a small amount of Cr(III). The displacement of Fe(II) by Cr(III) suggests that Cr(III) is adsorbing to the zeolite, rather than precipitating. Since the amount of adsorbed Fe(II) or Cr(III) are about the same when quantified as equivalents of charge, displacement of Fe(II) by Cr(III) can be

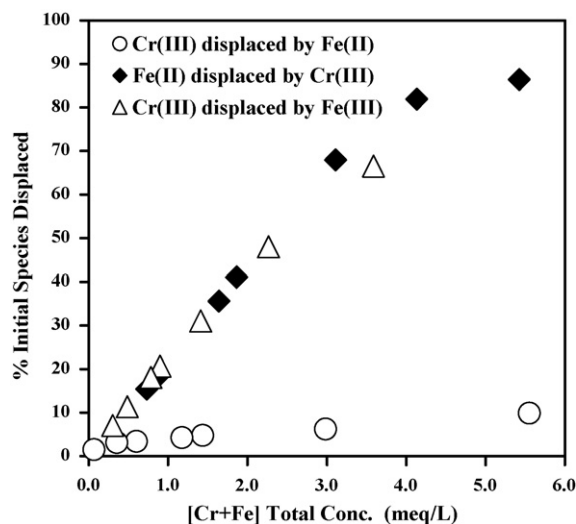


Fig. 3. Competitive exchanges on faujasite using sequential treatments of Cr(III) followed by Fe(II), Fe(II) followed by Cr(III), and Cr(III) followed by Fe(III).

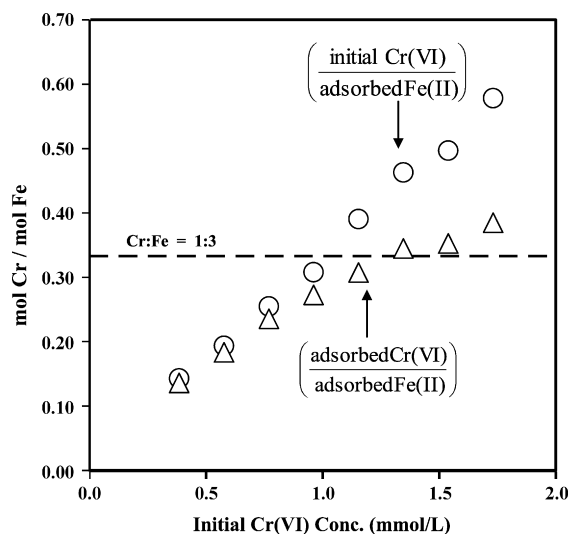
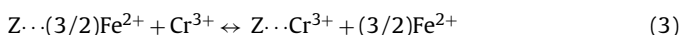


Fig. 4. Uptake of Cr(VI) by Fe(II)-treated zeolite. The initial adsorbed Fe(II) concentration is 1.05 mmol/g. Data have been normalized to the amount of adsorbed Fe(II). Initial Cr is the total added Cr(VI). At low [Cr(VI)], adsorbed Cr tracks available Cr. At higher [Cr(VI)], available Fe(II) limits the uptake near a Cr:Fe ratio of 1:3 (see Eq. (4)).

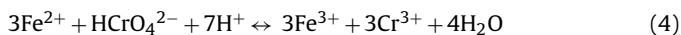
approximately described by



where $Z \cdots$ represents a zeolite cation exchange site. As shown in Fig. 3, the sequential addition of Fe(III) effectively displaces Cr(III). However, in subsequent experiments where oxidation of Fe(II) to Fe(III) by Cr(VI) occurred, minimal dissolved Fe or Cr were detectable suggesting that either (a) there were adequate zeolite exchange sites available for both Cr^{3+} and Fe^{3+} cation adsorption or (b) precipitation of Fe(III)/Cr(III) hydroxides had occurred.

3.2. Cr(VI) uptake by Fe(II)-treated faujasite

Measured Cr(VI) uptake at varying initial Cr(VI) concentrations (expressed as a mole ratio, [adsorbed Cr]:[adsorbed Fe]) is shown in Fig. 4. The mole ratio of (available Cr)/(adsorbed Fe) is also plotted to provide a reference. The removal of Cr(VI) by Fe(II)-faujasite reached a maximum solid loading of ~ 0.30 mmol Cr/g Fe(II)-faujasite ($\sim 1.5\%$ Cr, w:w). Uptake of Cr(VI) by Fe(II)-treated faujasite correlated directly with the measured amount of adsorbed Fe(II), with an observed Cr/Fe ratio close to 1:3 (Fig. 4). This result is consistent with the stoichiometry of the redox reaction:



At initial Cr(VI) treatment concentrations ≤ 0.80 mM the Cr(VI) uptake is directly proportional to added (initial) Cr(VI) under the experimental conditions (50 mg solid in 20 mL solution). However, at higher dissolved Cr(VI) (≥ 0.80 mM) the fixed amount of adsorbed Fe(II) limits the amount of Cr(VI) uptake when the Cr:Fe mole ratio in the system is greater than or equal to 1:3. Below Cr:Fe = 1:3 excess Fe(II) is present and Cr(VI) uptake is nearly complete. Above Cr:Fe = 1:3 there is excess Cr(VI) and Cr(VI) uptake levels off.

The reduction of Cr(VI) by Fe(II) is thermodynamically favorable and the results shown in Fig. 4 are consistent with previous work suggesting that Cr(VI) is reduced to Cr(III) followed by precipitation [15,16,22,23,26–28]. In addition, substantial evidence now suggests that Fe(II) is the predominant reducing agent generated during corrosion of metallic Fe [44,45]. The redox and adsorption reactions (Eqs. (3) and (4)) favor the formation of products so their coupling should mutually enhance reactivity; the Cr(III) product of Eq. (4) is a reactant for Eq. (3). Hypothetically, Fe(II) adsorbed

at sites inaccessible to Cr(VI) within the faujasite crystal structure could be displaced by Cr(III) (or Fe(III)) redox products and then would be available for reaction with dissolved Cr(VI). Additionally, solid surfaces such as silica and goethite have been shown to enhance the rate of reaction of Fe(II) with Cr(VI) [30] and the Fe(II)-faujasite may have similar surfaces.

3.3. SEM-EDX and XRD analyses

The results of SEM imaging showed faujasite particles with a blocky, angular morphology with uniform sizes (~ 400 – 500 nm width by ~ 600 – 800 nm length) (Fig. 5A). The faujasite particle morphology remained intact during and after the Fe(II) and Cr(VI) treatments. Elemental analysis by EDX suggested that pure faujasite was free of Fe contaminants (Fig. 5A) and the Fe(II)-faujasite gave measurable Fe $K\alpha_1$ and $K\beta_1$ peaks at 6.40 and 7.06 keV, respectively (Fig. 5B). Some evidence can be seen for formation of a fine, nano-scale precipitate in the Cr(VI)-treated Fe(II)-faujasite sample associated with the surfaces of faujasite particles (Fig. 5C). This feature was probed by EDX spectroscopy, however the length scale was too small for EDX elemental mapping and thus it remains unclear if this feature is pure Fe(III) or Cr(III) hydroxide, or if a mixed Fe(III)–Cr(III) hydroxide is present. Both Fe $K\alpha_1$ and $K\beta_1$ peaks and Cr $K\alpha_1$ and $K\beta_1$ peaks (at 5.41 and 5.95 keV, respectively) were detected. The relative Fe and Cr EDX peak intensities corresponded well with previously measured solid Fe and Cr concentrations measured in batch experiments. The results of XRD analysis (Fig. 6) indicated that no alteration in the crystal structure of faujasite occurred, nor were any new crystalline phases detected. This suggests that if a mixed phase such as $Cr_xFe_{1-x}(OH)_3$ product is present that it is amorphous or poorly ordered.

3.4. XANES analysis

Cr K -edge XANES results indicate that Cr(VI) was reduced to Cr(III) by Fe(II)-faujasite (Fig. 7). A reference Na_2CrO_4 solution, metallic Cr foil, $CrCl_3$ solution, and Cr(III)-treated faujasite were also analysed. The reduction of Cr(VI) to Cr(III) can be inferred by both the absence of the strong pre-edge absorption peak characteristic of Cr(VI), along with the position of the K -edge. In tetrahedral Cr(VI) the pre-edge peak at 5994.5 eV is attributed to a symmetry-allowed transition of a 1s electron to a t_2^* antibonding orbital [22,24]. The Cr(VI) pre-edge peak is not present in the $CrCl_3$ reference solution or Cr(III)-treated faujasite sample. The Cr(III) samples show a weak pre-edge absorption feature at 5992.5 eV associated with transitions of 1s electrons to antibonding orbitals with octahedral symmetry [46]. The XANES spectrum for Cr(VI)-treated Fe(II)-faujasite retains a weak absorption peak at 5994.5 eV from the Cr(VI) pre-edge feature indicative of a trace amount ($\sim 1\%$) unreacted Cr(VI). Aside from the small Cr(VI) contribution, the XANES data for the Cr(VI)+Fe(II)-faujasite reaction suggest the product is predominantly Cr(III). Though some similarities to Cr(III)-treated faujasite are evident, the Cr(VI)-treated Fe(II)-faujasite XANES spectrum exhibits differences from the pure Cr(III)-faujasite sample such as a slight broadening of the main XANES peak centered at 6011 eV as well as different post-edge features detectable in the EXAFS region.

3.5. EXAFS analysis

EXAFS spectroscopy was employed to determine the local atomic structure of Cr in Cr(VI)-treated Fe(II)-faujasite. The experimental and fitted EXAFS Fourier transforms (radial structure functions) of Cr K -edge EXAFS spectra for 20.0 mM Na_2CrO_4 , Cr(VI)-treated goethite (α -FeOOH), and the faujasite samples are shown

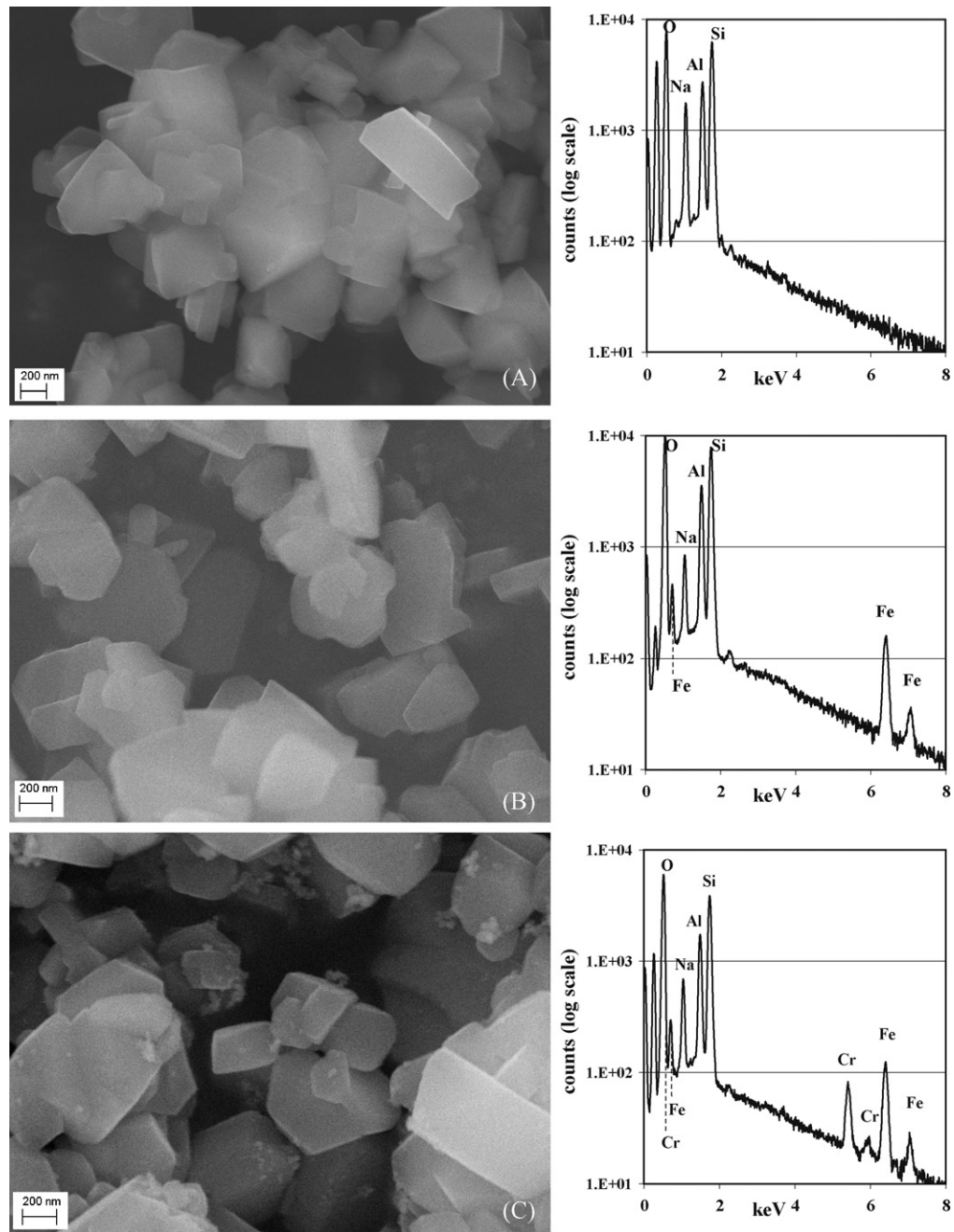


Fig. 5. SEM images with corresponding EDX spectra of (A) untreated faujasite, (B) Fe(II)-treated faujasite, and (C) Fe(II)-faujasite after reaction with Cr(VI). The Cr solid concentration in (C) is 0.28 mmol/g.

Table 1

Cr K-edge EXAFS fitting results from SIXPACK for Cr(VI) solution, Cr(VI)-treated goethite (α -FeOOH), Cr(III)-treated faujasite, and Cr(VI)-treated Fe(II)-faujasite.

Sample	Cr concentration	Shell	$(S_0^2)^a$	N	E_0 (eV)	R (\AA) ^b	σ^2 (\AA^2)	Goodness of fit (%) ^c
Na ₂ CrO ₄ solution	20.0 mM	Cr–O	0.80	4.00	0.65	1.66	0.002	7.8
		Cr–O	0.75	4.00	–1.36	1.64	0.0009	17
Cr(III)-faujasite	1.00 mmol g ⁻¹	Cr–Fe	0.75	1.50	–1.36	3.37	0.0009	20
		Cr–O	0.72	6.00	0.45	1.98	0.002	
		Cr–Cr	0.72	0.40	0.45	3.11	0.008	
Cr(VI)-treated Fe(II)-faujasite	0.28 mmol g ⁻¹	Cr–Si	0.72	1.80	0.45	3.51	0.001	25
		Cr–O	0.60	6.00	3.94	1.98	0.002	
		Cr–Cr ₁	0.60	1.00	3.94	3.13	0.002	

^a The amplitude reduction factor (S_0^2) was set at 0.8 during initial fitting and then allowed to vary as a final fitting step; N = coordination number (fixed during the fitting procedure); E_0 = Fermi shift; R = inter-atomic distance; σ^2 = Debye–Waller factor.

^b Errors in fitted R values estimated in SIXPACK were ± 0.02 \AA .

^c Goodness of fit parameter = $\text{Fit}(\%) = \frac{\sum(\chi_{\text{exp}} - \chi_{\text{fit}})^2}{\sum(\chi_{\text{exp}})^2} \times 100$ where χ_{exp} and χ_{fit} are the experimental and calculated $\chi(k)$ function data, respectively.

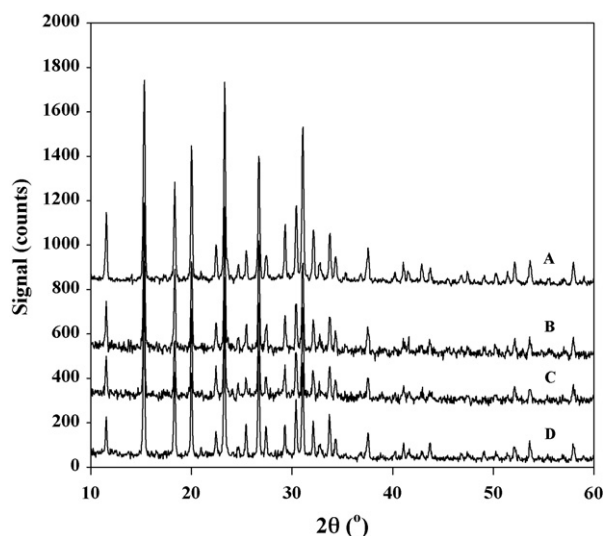


Fig. 6. X-ray diffraction patterns of (A) Na-faujasite, (B) Fe(II)-faujasite, (C) Cr(III)-faujasite, and (D) Cr(VI)-treated Fe(II)-faujasite. The data have been offset for clarity.

in Fig. 8 and the fitted values are given in Table 1. The results of Cr(VI)-treated goethite (α -FeOOH) have been included for comparison of the Cr–O inter-atomic distance of Cr(VI) with Cr(III). The Cr(VI)-treated α -FeOOH sample yielded a first Cr–O shell composed of four O atoms at an inter-atomic distance of $R = 1.66(\pm 0.02)$ Å (Table 1) which is comparable to 1.69 Å reported in previous Cr EXAFS studies [22,25]. A second backscattering Cr–Fe shell peak was used in the fit and included 1.5 Fe atoms at an inter-atomic distance of $R = 3.37(\pm 0.02)$ Å. The Cr–Fe second shell at 3.37 Å sug-

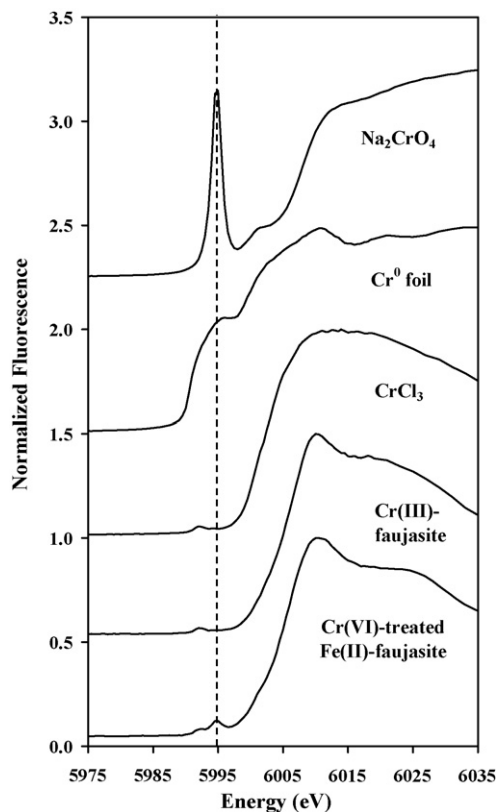


Fig. 7. Normalized Cr *K*-edge XANES for Cr(VI)-treated Fe(II)-faujasite and various reference compounds. The vertical dashed line at 5994.5 eV corresponds to the Cr(VI) pre-edge feature described in the text. The data have been offset for clarity.

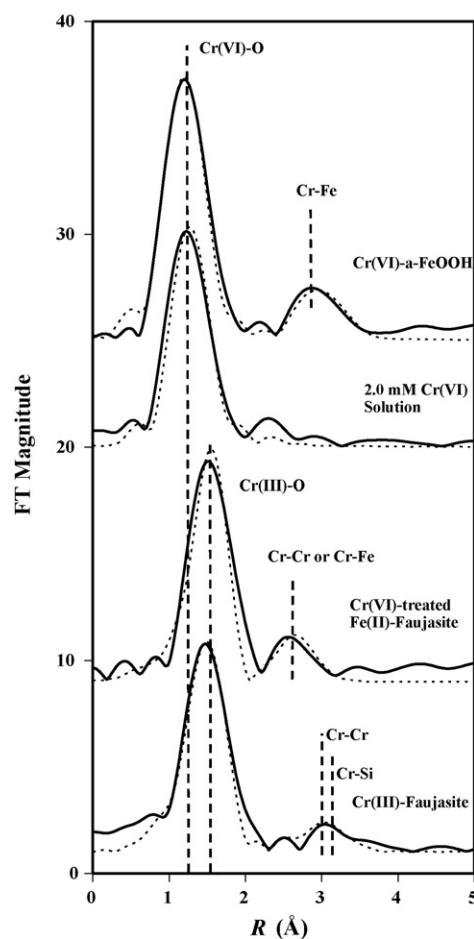


Fig. 8. Cr *K*-edge EXAFS Fourier-transformed experimental spectra (solid lines) and theoretical fits from Sixpack software (dashed lines). All data are uncorrected for phase shift. From top to bottom: Cr(VI)-treated goethite (α -FeOOH), Na_2CrO_4 in 2.0 mM aqueous solution, Cr(VI)-treated Fe(II)-faujasite, and Cr(III)-treated faujasite.

gests that the CrO_4^{2-} anion binds directly to the α -FeOOH surface by an inner-sphere adsorption mechanism [47,48].

The Cr *K*-edge EXAFS data for Cr(III)-treated faujasite were included to compare the local atomic environment of Cr(III) adsorbed on untreated zeolite with Cr(III) produced from Cr(VI) reduction by Fe(II). Both Cr(III)-treated faujasite and Cr(VI)-treated Fe(II)-faujasite show a coherent Cr–O shell of six O atoms at $R = 1.98(\pm 0.02)$ Å. This *R* value agrees well a Cr–O distance of 1.99 Å found in previous EXAFS work on synthetic $\text{Cr}(\text{OH})_3 \cdot n\text{H}_2\text{O}$ precipitate [49], Cr(III) adsorption complexes on hydrous Fe(III) oxides [47], and Cr(III) surface precipitates on silica [48].

Second shell peaks at distances greater than 1.99 Å were also fit and ascribed to backscattering from shells of metal atoms (Cr–Cr, Cr–Fe, or Cr–Si) beyond the Cr–O shell (Fig. 8). The Cr(III)-treated faujasite contained no Fe and the spectrum shows distinct differences from the Cr(VI)-treated Fe(II)-faujasite sample. Most notable is the presence of a peak at 3.51 Å ascribed to Cr–Si which is absent in the Cr(VI)-treated Fe(II)-faujasite sample. In the case of Cr(VI)-treated Fe(II)-faujasite, either Cr–Fe or Cr–Cr shells were successfully used to describe the second shell since EXAFS cannot discern differences in the atomic number (*Z*) of nearest neighbors that are $Z \pm 2$ [25]. A reasonable fit to the Cr(VI)-treated Fe(II)-faujasite was determined using a Cr–O shell at 1.98 Å ($N = 6$) and a Cr–(Cr,Fe) shell at $R = 3.13(\pm 0.02)$ Å ($N = 1$) (Table 1). These inter-atomic distances agree well with previous investigations of Cr(III) surface precipitation on silica [46] and hydrous ferric oxide [45].

Based on EXAFS results it can be reasonably assumed that the Cr^{3+} cation is binding to the aluminosilicate cation exchange site of the faujasite cage structure in the Cr(III) -faujasite sample whereas the Cr^{3+} cation in the Cr(VI) -treated Fe(II) -faujasite is closely associated with other Cr^{3+} or Fe^{3+} cations in a poorly ordered precipitate. Formation of amorphous, mixed phase precipitates such as $\text{Cr}_x\text{Fe}_{1-x}(\text{OH})_3$ have been previously reported in the solid product mixtures after reaction of Cr(VI) with Fe(II) and Fe^0 [15,16,22,23,26–28]. The porosity and 7.4 Å effective channel width [40] of faujasite suggests that an $\text{Cr}_x\text{Fe}_{1-x}(\text{OH})_3$ product could form both on the exterior faujasite particle surfaces (see Fig. 5C) or within channels of the faujasite frame network.

4. Implications for Cr(VI) remediation

Untreated zeolites exhibit little or no affinity for Cr(VI) . However, their ability to adsorb Fe(II) provides an effective means for delivering this reactant for subsequent reduction of Cr(VI) to Cr(III) . The reduction of Cr(VI) by Fe(II) is favorable under environmentally relevant conditions and this study indicates that Fe(II) adsorbed by faujasite is accessible for the Cr(VI) reduction reaction. Since Cr(III) (the product of Cr(VI) reduction) readily displaces Fe(II) from the faujasite exchange sites a cooperative mechanism between these two favorable reactions occurs where generation of Cr(III) results in cation exchange with Fe(II) causing more Cr(VI) reduction by Fe(II) . Furthermore, the presence of the Al-Si-O and SiO_2 surfaces in the faujasite structure may assist the reaction of Cr(VI) with Fe(II) by providing a catalytic effect.

Further steps are needed before field application of Fe(II) -treated zeolite. For example, though faujasite is well-characterized and contains minimal impurities, this synthetic zeolite would not be cost effective on a field scale. Field application would more likely use natural zeolite available as an industrial-scale sorbent. Column studies are also necessary to determine the efficiency of Cr(VI) reduction under dynamic, flow-through conditions are needed. The results of this study suggest that Fe(II) -treated zeolites are effective in removing Cr(VI) from aqueous solution, either alone or perhaps as a co-additive in Fe^0 -based remediation.

Acknowledgements

We appreciate the assistance of Matt Newville (APS-GSECARS) who assisted our XAS setup and data collection, Hanchool Kwon (University of Illinois, Urbana-Champaign) who helped with XAS data collection, and Sam Webb (SSRL) for help on SIXPACK EXAFS data analysis. The XAS measurements were collected at GSECARS (Sector 13, APS), Argonne National Laboratory, which is supported by the NSF (EAR-0217473), the U.S. DOE (DE-FG02-94ER1466), and the State of Illinois. Support for this work was provided by the Research Corporation Cottrell College Science Program (Awards CC6462 and CC5444) and the National Science Foundation Major Research Instrumentation (NSF-MRI) program (Awards CHE-0421285 and CHE-0821619).

References

- [1] S.A. Katz, H. Salem, *The Biological and Environmental Chemistry of Chromium*, VCH, New York, 1994.
- [2] U.S. EPA. Field Applications of in situ remediation technology: Permeable reactive barriers; Environmental Protection Agency. EPA 542-R-99-002. Washington, DC 20460. December 1999.
- [3] M.E. Losi, C. Amrhein, W.T. Frankenberger, Factors affecting chemical and biological reduction of hexavalent chromium in soil, *Environ. Toxicol. Chem.* 13 (1994) 1727–1735.
- [4] M.A. Stewart, P.M. Jardin, C.C. Brabdt, M.O. Barnett, S.E. Fendorf, L.D. McKay, T.L. Mehlhorn, K. Paul, Effects of contaminant concentration, aging, and soil properties on the bioaccessibility of Cr(III) and Cr(VI) in soil, *Soil Sediment Contamin.* 12 (2003) 1–21.
- [5] M. Zupančič, M. Zupančič Justin, P. Bukovec, V.S. Šelih, Chromium in soil layers and plants on closed landfill site after landfill leachate application, *Waste Manage.* 29 (2009) 1860–1869.
- [6] C.H. Jung, T. Matsuto, N. Tanaka, Flow analysis of metals in a municipal solid waste management system, *Waste Manage.* 26 (2006) 1337–1348.
- [7] C.-J. Cheng, T.-H. Lin, C.-P. Chen, K.-W. Juang, D.-Y. Le, The effectiveness of ferrous iron and sodium dithionite for decreasing resin-extractable Cr(VI) in Cr(VI) -spiked alkaline soils, *J. Hazard. Mater.* 164 (2009) 510–516.
- [8] R.J. Bartlett, J.M. Kimble, Behavior of chromium in soils: I. Trivalent forms, *J. Environ. Qual.* 5 (1976) 379–383.
- [9] R.J. Bartlett, J.M. Kimble, Behavior of chromium in soils: II. Hexavalent forms, *J. Environ. Qual.* 5 (1976) 383–386.
- [10] T.K. Tokunaga, J. Wan, M.K. Firestone, T.C. Hazen, K.R. Olson, D.J. Herman, S.R. Sutton, A. Langzirotti, In situ reduction of chromium(VI) in heavily contaminated soils through organic carbon amendment, *J. Environ. Qual.* 32 (2003) 1641–1649.
- [11] D.Y. Lee, J.C. Huang, K.W. Juang, L. Tsui, Assessment of phytotoxicity of chromium in flooded soils using embedded selective ion exchange resin method, *Plant Soil* 277 (2005) 97–105.
- [12] U.S. EPA. Development document for the proposed effluent limitations guidelines and standards for the metal products & machinery point source category. Environmental Protection Agency. EPA-821-B-00-005. Washington, DC 20460. December 2000.
- [13] J.P. Gould, The kinetics of hexavalent chromium reduction by metallic iron, *Water Res.* 16 (1982) 871–877.
- [14] R.M. Powell, R.W. Puls, S.K. Hightower, D.A. Sabatini, Coupled iron corrosion and chromate reduction-mechanisms for subsurface remediation, *Environ. Sci. Technol.* 29 (1995) 1913–1922.
- [15] A.R. Pratt, D.W. Blowes, C.J. Ptacek, Products of chromate reduction on proposed subsurface remediation material, *Environ. Sci. Technol.* 31 (1997) 2492–2498.
- [16] D.W. Blowes, C.J. Ptacek, J.L. Jambor, In-situ remediation of Cr(VI) -contaminated groundwater using permeable reactive walls: laboratory studies, *Environ. Sci. Technol.* 31 (1997) 3348–3357.
- [17] R.W. Puls, C.J. Paul, R.M. Powell, The application of in situ permeable reactive (zerovalent iron) barrier technology for the remediation of chromate-contaminated groundwater: a field test, *Appl. Geochem.* 14 (1999) 989–1000.
- [18] T. Astrup, S.L.S. Stipp, T.H. Christensen, Immobilization of chromate from coal fly ash leachate using an attenuating barrier containing zero-valent iron, *Environ. Sci. Technol.* 34 (2000) 4163–4168.
- [19] N. Melitas, O. Chuffe-Moscoco, J. Farrell, Kinetics of soluble chromium removal from contaminated water by zerovalent iron media: corrosion inhibition and passive oxide effects, *Environ. Sci. Technol.* 35 (2001) 3948–3953.
- [20] S. Gandhi, B.T. Oh, J.L. Schnoor, P.J.J. Alvarez, Degradation of TCE, Cr(VI) , sulfate, and nitrate mixtures by granular iron in flow-through columns under different microbial conditions, *Water Res.* 36 (2002) 1973–1982.
- [21] R.T. Wilkin, C.M. Su, R.G. Ford, C.J. Paul, Chromium-removal processes during groundwater remediation by a zerovalent iron permeable reactive barrier, *Environ. Sci. Technol.* 39 (2005) 4599–4605.
- [22] B.A. Manning, J.R. Kiser, H.C. Kwon, S.R. Kanel, Spectroscopic investigation of Cr(III) - and Cr(VI) -treated nanoscale zerovalent iron, *Environ. Sci. Technol.* 41 (2007) 586–592.
- [23] J. Cao, W.-X. Zhang, Stabilization of chromium ore processing residue (COPR) with nanoscale iron particles, *J. Hazard. Mater.* 132 (2006) 213–219.
- [24] S.E. Fendorf, G.C. Li, Kinetic of chromate reduction by ferrous iron, *Environ. Sci. Technol.* 30 (1996) 1614–1617.
- [25] R. Patterson, S. Fendorf, Reduction of hexavalent chromium by amorphous iron sulfide, *Environ. Sci. Technol.* 31 (1997) 2039–2044.
- [26] L.E. Eary, D. Rai, Chromate removal from aqueous wastes by reduction with ferrous ion, *Environ. Sci. Technol.* 22 (1988) 972–977.
- [27] Z. Li, H.K. Jones, R.S. Bowman, R. Helfferich, Enhanced reduction of chromate and PCE by palletized surfactant-modified zeolite/zerovalent iron, *Environ. Sci. Technol.* 33 (1999) 1291–1298.
- [28] S.M. Ponder, J.G. Darab, T.E. Mallouk, Remediation of Cr(VI) and Pb(II) aqueous solutions using supported, nanoscale zero-valent iron, *Environ. Sci. Technol.* 34 (2000) 2564–2569.
- [29] S. Hug, H. Haubscher, Iron(III) catalyzed photochemical reduction of chromium(VI) by oxalate and citrate in aqueous solutions, *Environ. Sci. Technol.* 31 (1997) 160–170.
- [30] I. Buerge, S. Hug, Influence of mineral surfaces on chromium(VI) reduction by iron(II), *Environ. Sci. Technol.* 33 (1996) 4285–4291.
- [31] S.E. Fendorf, Surface reactions of chromium in soils and waters, *Geoderma* 67 (1995) 55–71.
- [32] D. Wu, Y. Sui, S. He, X. Wang, C. Li, H. Kong, Removal of trivalent chromium from aqueous solution by zeolite synthesized from coal fly ash, *J. Hazard. Mater.* 155 (2008) 415–423.
- [33] B. Liguori, A. Cassese, C. Colell, Safe immobilization of Cr(III) in heat-treated zeolite tuff compacts, *J. Hazard. Mater.* 137 (2006) 1206–1210.
- [34] V.J. Inglezakis, M.D. Loizidou, H.P. Grigoropoulou, Ion Exchange of Pb^{2+} , Cu^{2+} , Fe^{3+} , and Cr^{3+} on natural clinoptilolite: selectivity determination and influence of acidity on metal uptake, *J. Colloid Interface Sci.* 261 (2003) 49–54.
- [35] M.V. Meir, R.L. Callejas, R. Gehr, B.E.J. Cisneros, P.J.J. Alvarez, Heavy metal removal with Mexican clinoptilolite: Multi-component ionic exchange, *Wat. Res.* 35 (2001) 373–378.
- [36] R. Leyva-Ramos, A. Jacobo-Azuara, P.E. Diaz-Flores, R.M. Guerrero-Coronado, J. Mendoza-Barron, M.S. Berber-Mendoza, Adsorption of chromium(VI) from

- an aqueous solution on a surfactant-modified zeolite, *Colloids and Surfaces A: Physicochemical and Engineering Aspects* 330 (2008) 35–41.
- [37] Z. Li, H.-K. Jones, R.S. Bowman, R. Helderich, Enhanced reduction of chromate and PCE by pelletized surfactant-sodified zeolite/zerovalent iron, *Environ. Sci. Technol.* 33 (1999) 4326–4330.
- [38] Z. Li, R.S. Bowman, Counterion effects on the sorption of cationic surfactant and chromate on natural clinoptilolite, *Environ. Sci. Technol.* 31 (1997) 2407–2412.
- [39] G.M. Haggerty, R.S. Bowman, Sorption of chromate and other inorganic anions by organo-zeolite, *Environ. Sci. Technol.* 28 (1994) 452–458.
- [40] D.W. Ming, F.A. Mumpton, Zeolites in soils, in: J.B. Dixon, S.B. Weed, R.C. Dinauer (Eds.), *Minerals in Soil Environments*, Soil Science Society of America, Madison, WI, 1989, pp. 873–911.
- [41] S.M. Webb, SIXPACK: a graphical user interface for XAS analysis using IFEFFIT, *Physica Scripta T115* (2005) 1011–1014.
- [42] M. Newville, IFEFFIT: interactive XAFS analysis and FEFF fitting, *J. Synchrotron Rad.* 8 (2001) 324–332.
- [43] J.J. Rehr, S.I. Zabinsky, R.C. Albers, High-order multiplescattering calculations of X-ray absorption fine structure, *Phys. Rev. Lett.* 69 (1992) 3397–3400.
- [44] C. Noubactep, A critical review on the mechanism of contaminant removal in $\text{Fe}^0\text{-H}_2\text{O}$ systems, *Environ. Technol.* 29 (2008) 909–920.
- [45] C. Noubactep, Processes of contaminant removal in “ $\text{Fe}^0\text{-H}_2\text{O}$ ” systems revisited the importance of co-precipitation, *Open Environ. J.* 1 (2007) 9–13.
- [46] I. Arcon, B. Mirtic, A. Kodre, Determination of valence states of chromium in calcium chromates by using X-ray absorption near-edge structure (XANES) spectroscopy, *J. Am. Ceram. Soc.* 81 (1998) 222–224.
- [47] L. Charlet, A.A. Manceau, X-ray absorption spectroscopic study of the sorption of Cr(III) at the oxide-water interface: II. Adsorption, coprecipitation, and surface precipitation on hydrous ferric oxide, *J. Colloid Interface Sci.* 148 (1992) 443–458.
- [48] S.E. Fendorf, G.M. Lamble, M.G. Stapleton, M.J. Kelley, D.L. Sparks, Mechanisms of chromium(III) sorption on silica. 1. Cr(III) surface structure derived by extended X-ray absorption fine structure spectroscopy, *Environ. Sci. Technol.* 28 (1994) 204–289.
- [49] A.A. Manceau, L. Charlet, X-ray absorption spectroscopic study of the sorption of Cr(III) at the oxide-water interface: I. Molecular mechanism of Cr(III) oxidation on Mn oxides, *J. Colloid Interface Sci.* 148 (1992) 425–442.